Use of a Static Magnetic Field in Measuring the Thermal Conductivity of a Levitated Molten Droplet

A.A. Roy, S. Easter, V. Bojarevics, K. Pericleous
School of Computing and Mathematical Sciences, University of Greenwich, London, UK

Abstract

Numerical models are used to analyze the complex behaviour of magnetically levitated droplets in the context of determining their thermophysical properties. We focus on a novel method reported in Tsukada et al. [4] which uses periodic laser heating to determine the thermal conductivity of an electromagnetically levitated droplet in the presence of a static DC field to suppress convection. The results obtained from the spectral-collocation based free surface code SPHINX and the commercial package COMSOL independently confirm and extend previous findings in [4]. By including the effects of turbulence and movement of the free surface SPHINX can predict the behaviour of the droplet in dynamic regimes with and without the DC magnetic field. COMSOL is used to investigate arbitrary amplitude axial translational oscillations when the spherical droplet is displaced off its equilibrium. The results demonstrate that relatively small amplitude oscillations could cause significant variation in Joule heating and redistribution of the temperature. The effect of translational oscillations on the lumped circuit inductance is analysed. When a fixed voltage drive is applied across the terminals of the levitation coil, this effect will cause the coil current to change and a correction is needed to the electromagnetic force acting on the droplet.

1. Introduction

There are many papers which deal with the measurement of highly reactive materials using electromagnetic levitation. The advantage of using levitation is that the specimen can be analysed in a contactless environment thereby avoiding interaction with the experimental apparatus which could compromise the measurement. From experimental observation of the oscillation frequency and damping rate of a levitated liquid droplet it is possible to calculate the viscosity and surface tension. Such experiments have been performed under terrestrial and micro-gravity conditions, eg. Egry et al. [1].

In this paper we investigate a technique developed originally by Wunderlich & Fecht [2] and later extended by Fukuyama et al [3] to measure the thermal conductivity of an electromagnetically levitated metallic droplet. The droplet is levitated in the high frequency AC field of a seven-turn coil (with the top two turns counter wound with respect to the lower turns) and its upper surface is exposed to periodic laser heating. A semi-analytical model developed by Tsukada et al. [4] shows how the phase shift between the input power and the temperature response at the bottom of the droplet depends on the thermal conductivity. The thermal conductivity is determined by relating the semi-analytical model to experimental measurements of the phase shift. Turbulent convective heat transfer in the droplet, driven by stirring electromagnetic forces, buoyancy and thermo-capillary effects disrupts the accuracy of the technique, which necessitates conducting the experiment in the presence of a strong homogeneous axially directed DC magnetic field to damp the velocity field. Tsukada et al [4] apply the technique to silicon (although its applicability to other materials has been demonstrated) and show that, for the case of a molten spherical Si droplet, a static magnetic field exceeding 4-5T in strength is sufficient to obtain an accurate measurement of the thermal conductivity. The physical properties of the molten silicon and operating conditions are listed in Table 1 and are retained for use in our own calculations. Fig. 1 shows the geometry of the experimental arrangement, ignoring the helicity of the inductor coils and the external connections.

Physical properties of molten silicon

Density [kg/m^3]	2530
Thermal conductivity [W/(mK)]	64
Emissivity [-]	0.3
Specific heat [J/(kgK)]	1000
Electrical conductivity [S/m]	1.2 x 10^6
Melting temperature [K]	1683
Operating conditions	
Electric current (amplitude) in RF coil [A]	375
Frequency of electric current in RF coil [kHz]	200
Laser power [W]	9.56
Ambient temperature [K]	323
Droplet diameter [m]	8 x 10^{-3}
e^{-2} radius of semiconductor laser beam	2 x 10^{-3}
Spot radius of pyrometer [m]	2 x 10^{-3}

Table 1 – Physical properties and operating conditions.

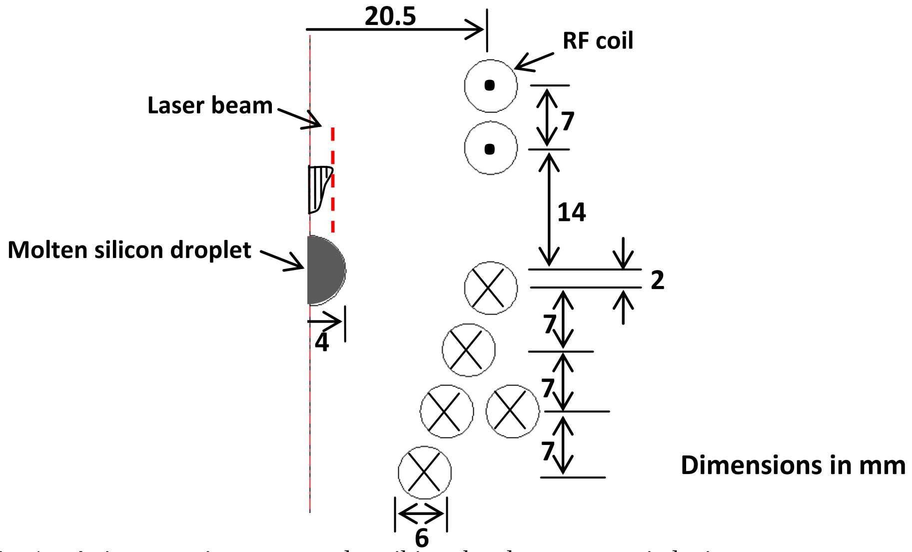

Fig. 1 – Axisymmetric geometry describing the electromagnetic levitator.

In this paper two sets of results are reported using (i) the commercial multiphysics package COMSOL [10] (Sec. 3.1) and (ii) the spectral-collocation based free surface code SPHINX [6] (Sec 3.2). Our aim is not to compare the performance of these packages but rather to extend the existing results in [4] reviewing possible effects which could disrupt the measurement and to investigate more realistic models with free-surface motion allowing for turbulence.

COMSOL has been used to describe the axial translational motion which results when the droplet is displaced off its equilibrium. Estimates of the change in Joule heating in the droplet suggest that even small amplitude oscillations could disrupt the temperature modulation state and prevent accurate measurement of the phase shift. If an RF voltage of fixed amplitude is maintained across the terminals of the coil, small changes in the position of the droplet could cause the current to deviate slightly.

The results obtained from SPHINX complement those produced by COMSOL but are more realistic and consider in addition the transient movement of the free surface and temperature dependent surface tension which induces thermo-capillary flow. SPHINX also models the effects of turbulence which permit numerical simulations situations when the DC field is not sufficiently strong to ensure laminar flow – a case not considered in [4]. Moreover, for DC magnetic fields of low to moderate strength, it appears that the turbulence generation is reduced and that large scale mixing grows up until a certain threshold beyond which it starts to decrease [9]. It is of interest to note that while the electromagnetically driven flow is reduced, the Marangoni effect still drives a flow of significant intensity along the free surface [4,9].

2. Modelling Approach

COMSOL is an FEA software package used for analysing coupled phenomena in physics and engineering applications. COMSOL is used herewith to describe the axisymmetric solution to the coupled system of differential equations governing the electromagnetic field (Maxwell's Equations), fluid flow (incompressible Navier Stokes) and heat transfer (conduction, convection and radiation) with the assumption that the droplet remains perfectly spherical. The electromagnetic solution provides the time-averaged Lorentz and Joule sources responsible for stirring and heating the fluid. Boundary conditions are applied via the user interface, including the choice of solver for each physics module which can be either transient or steady state. The mesh is generated automatically but can be refined locally to allow accurate field resolution of the skin effect in the coils and droplet – see Fig. 2. The steady state electromagnetic vector potential is solved throughout the entire domain but the transient velocity, pressure and temperature fields (which are adjusted by the presence of the laser) are only solved in the subdomain representing the droplet.

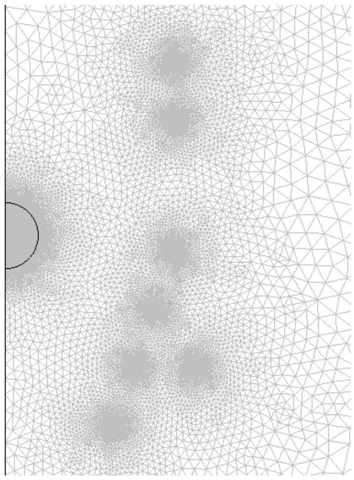

Fig. 2 – The mesh used in the axisymmetric FEA solution (COMSOL).

While COMSOL uses standard laminar flow equations, the SPHINX code computes the numerical solution of the turbulent momentum and heat transfer equations for an incompressible fluid:

$$\rho\left(\frac{\partial \mathbf{v}}{\partial t}+(\mathbf{v}.\nabla)\mathbf{v}\right)=-\nabla p+\nabla.(\rho\nu_e(\nabla\mathbf{v}+\nabla\mathbf{v}^T))+\mathrm{Re}(\boldsymbol{J}\times\boldsymbol{B}^*)/2+\rho\boldsymbol{g} \tag{1}$$

$$\nabla.\mathbf{v}=0 \tag{2}$$

$$\rho C_p\left(\frac{\partial T}{\partial t}+\mathbf{v}.\nabla T\right)=\nabla.(\rho C_p\alpha_e\nabla T)+\mathrm{Re}(\boldsymbol{E}.\boldsymbol{J}^*)/2 \tag{3}$$

where $\mathbf{v}$ is the velocity vector, p - the pressure, ρ - the density, ν_e is the effective viscosity (computed from the 2-equation k-ω model with magnetic damping terms [5]), Re($\boldsymbol{J}$x$\boldsymbol{B}$*)/2 is the time-averaged electromagnetic force, $\boldsymbol{g}$ - the gravity vector, T - the temperature, α_e - the effective thermal diffusivity (related to ν_e), C_p - the specific heat, and Re($\boldsymbol{E}.\boldsymbol{J}$*)/2 is the time-averaged Joule heat. The implementation of the k-ω turbulence model, including the effect of magnetic damping is described in [5, 9]. The boundary conditions at the external free surface are stated in terms of the hydrodynamic stress tensor and the interface position $\boldsymbol{R}(t)$ moves continuously according to the calculated material velocity $\mathbf{v}(t)$:

$$\Pi_{nn} = \gamma K \qquad \Pi_{n\tau} = \gamma_T \nabla T . \mathbf{e}_\tau \qquad \mathbf{e}_\mathbf{n} . \mathbf{v} = \mathbf{e}_\mathbf{n} . \partial_t \mathbf{R} \tag{4}$$

where the subscripts n, τ correspond to projections onto $\mathbf{e}_n$ and $\mathbf{e}_\tau$ - the normal and tangential unit vectors at the free surface, $\gamma(T)$ is the temperature dependent surface tension coefficient, K - the local mean curvature.

While the droplet radiates heat to the ambient surroundings a Gaussian distributed influx of heat (supplied by the laser) is imposed on its upper surface. The thermal boundary conditions are therefore given by

$$-\mathbf{e}_{\boldsymbol{n}} . (-k \nabla T) = q_{laser} + \varepsilon \sigma (T_{amb}^4 - T^4), \tag{5}$$

$$q_{laser} = \alpha \, 2 P_0 / (\pi \, r_{laser}^2)(1 + \cos \omega_{laser} \, t) \exp(-2 r^2 / r_{laser}^2)(\mathbf{e}_{\boldsymbol{n}} . \mathbf{e}_{laser}) ,$$

where r_{laser} is the radius at which the laser intensity is less by a factor of e^2, ω_{laser} is the angular frequency of the beam, α_p is the absorptivity, the intensity of the laser beam at the centreline is related to the beam power P_0. The results contained in [3,4] use a beam with P_0=9.56W, r_{laser} = 0.002 m, $f_{laser} = \omega_{\text{laser}}/2\pi$ = 0.1Hz is used.

The axisymmetric form of Eqns. 1-3 are solved in spherical coordinates using a spectral-collocation method where the velocity vector components and pressure are represented as series of Chebyshev polynomials and Legendre functions. A more detailed description of the mathematical model is given in Bojarevics & Pericleous [6]. The mesh is initially spherical; Fig. 3 shows the typical shape to which it will deform at a particular instant in time after adjusting to the magnetic pressure from the surrounding coils.

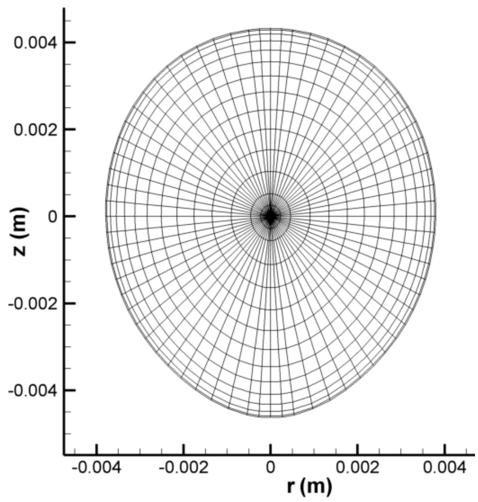

Fig. 3 – The mesh used in the SPHINX simulations.

3. Numerical results using COMSOL

Three sets of results are presented in this section. First we confirm some of the results presented in [3,4] and show how the phase of the temperature waveform at the bottom of the droplet varies with the thermal conductivity when laser modulated heating is applied (Sec. 3.1). Next we examine the force on the droplet when its position on the symmetry axis of the coils is varied and investigate axial translational oscillations (Sec. 3.2). Finally we investigate how the motion of the droplet could affect the lumped electrical circuit impedance (Sec. 3.3).

3.1 Comparison of results with Tsukada et al.

Tsukada et al. [4] report results on temperature/fluid flow in the droplet for the case when the laser is absent. Assuming the same geometry, material properties and operating conditions in [4] these results have been closely replicated with COMSOL.

The COMSOL solution in Fig. 4 shows a scalar plot of $|\boldsymbol{B}|$ and streamlines of magnetic flux. The current is confined to a thin skin and concentrates on the inner surfaces of the coils where the contours are tightly bunched. The highest values of $|\boldsymbol{B}|$ are found in the space enclosed by the bottom coil turn which has the smallest radius and leads to higher flux confinement. Fig. 5 shows scalar plots of v_z and temperature in the droplet when a uniform DC magnetic field of 4T is applied. The results closely match, qualitatively and quantitatively, those produced in [4]; two circulating vortices are present and the highest temperatures form a circular plateau in the lower half of the droplet.

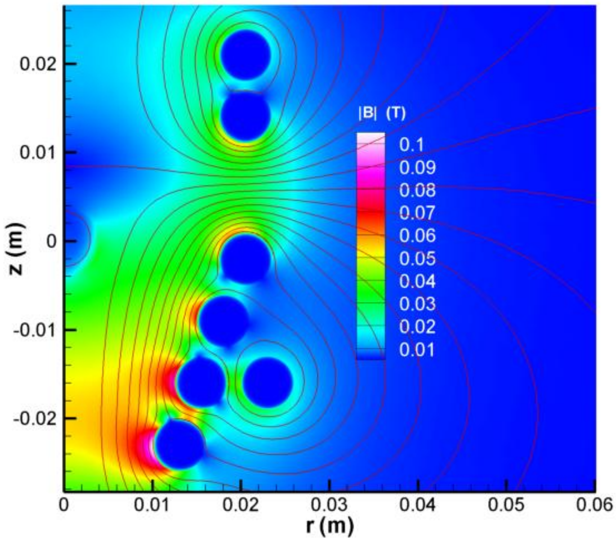

Fig. 4 – COMSOL model of electromagnetic levitator (f=200 kHz, I_{peak} = 375A).

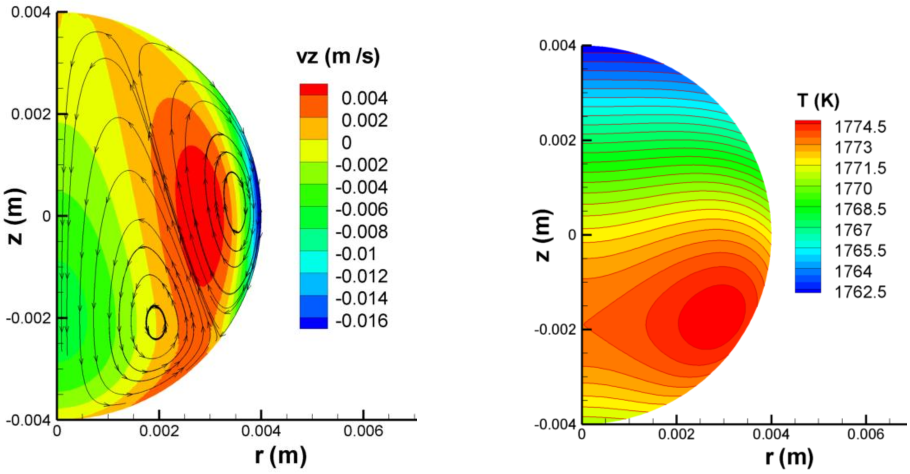

Fig. 5 – Scalar plots of v_z and temperature in the spherical droplet (COMSOL).

Our solution permits analysis of the loop voltage phasors $\overline{V}_i$ (i = 1,2...,7) associated with each turn of the coil. These phasors are listed in Table 2 (from top to bottom) and are determined from the relationship V=ZI where Z is the [7x7] complex impedance matrix and I is the imposed [7x1] current vector. The top two turns of the coil have the opposite sign to the lower set since they enclose flux which is oppositely directed. The net voltage across the terminals of the supply, ignoring the drop due to coil helicity and external connections, is obtained by adding the phasors together (with some sign adjustment according to the direction of the current). The net voltage is therefore $\bar{V}_{net} = -4.623 - 241.58\mathrm{i}$ implying a peak amplitude of 241.62V. Since the imposed current is $\bar{I} = 375 + 0\,\mathrm{i}$ the total power dissipated is $\mathrm{Re}(VI^*)/2 =$ 866.81W. This value agrees well (differing by less than 0.5%) with the volume integral $\iiint \mathrm{Re}(E.J^*)/2\,dV$ over all the conducting regions indicating that the model is self-consistent.

Coil turn (top to bottom)	Voltage phasor
1	0.4727+26.635i
2	0.2724+23.465i
3	-0.693-36.821i
4	-0.943-41.574i
5	-0.746-38.010i
6	-1.217-47.608i
7	-0.279-27.466i

Table 2 – Phasors describing the loop voltages in the coils.

Tsukada et al. [4] report the variation in phase shift according to the choice of thermal conductivity when the laser frequency is 0.1 Hz. These results have been reproduced with COMSOL. Fig. 6 (left) shows the temperature modulation state at the bottom of the droplet over one cycle of laser heating (see Eqn. 6) with f_{laser}=0.1 Hz for various thermal conductivities $k=\alpha\rho C_p$. Fig. 6 (right) shows how the phase shift between these waveforms and that of the laser (which is taken as the reference) depends on the choice of k. The phase shift becomes less as the value of k is increased. Excellent agreement was obtained between these results and those given in [4].

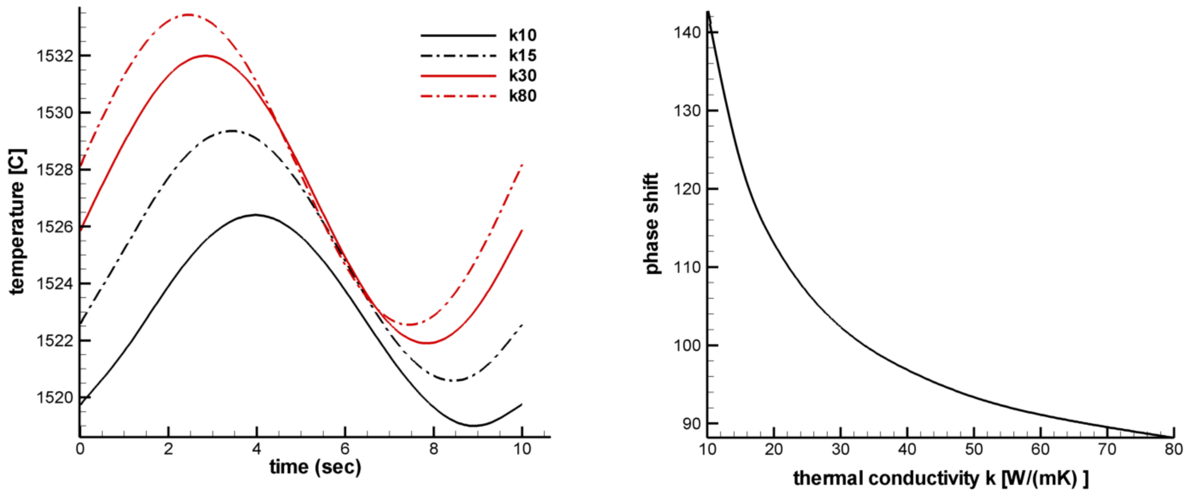

Fig. 6 – Temperature modulation state (left) and phase shift as a function of k (right) when f_{laser}=0.1Hz (COMSOL).

3.2 Axial translational oscillations

Fig. 7 shows how the (time-averaged) axial force on the droplet $\int \mathrm{Re}(B_r J_\phi^*)/2\,dV - mg$ varies according to its z-position on the symmetry axis of the coils, with and without the influence of gravity. The zero-crossings of the curves indicate positions where the force is balanced. In earthbound conditions there is one stable and unstable equilibrium, whereas in zero-gravity there is one stable and two unstable equilibria. The equilibria are indicated by the red (stable) and black (unstable) circles.

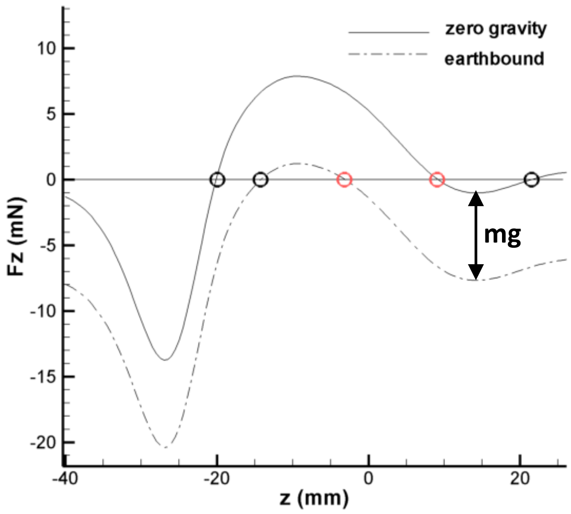

Fig. 7 – The axial force on the droplet as a function of z.

The results in Fig. 7 can be used to generate phase space portrait diagrams in (z,v_z) space describing the motion when the droplet is displaced off its equilibrium. This is achieved by fitting a spline through the graphs and applying a standard ode solver to evolve the following pair of differential equations forward and backwards in time:

$$\frac{dv_z}{dt} = \frac{F_z(z)}{m} - g$$
$$\frac{dz}{dt} = v_z$$

Phase space portraits for earthbound and zero gravity conditions are given in Fig. 8. Most of the orbits were produced using appropriately chosen initial conditions $z=z_{in}$, $v_z=0$ around the region of interest. The closed curves indicate oscillatory motion around the stable equilibria while the dotted curves represent "fly-by" trajectories where the droplet is temporarily caught in the field of the coils but does not remain permanently bound. The unstable equilibria are associated with hyperbolic fixed points whose stable and unstable manifolds are indicated by the blue and red arrows respectively.

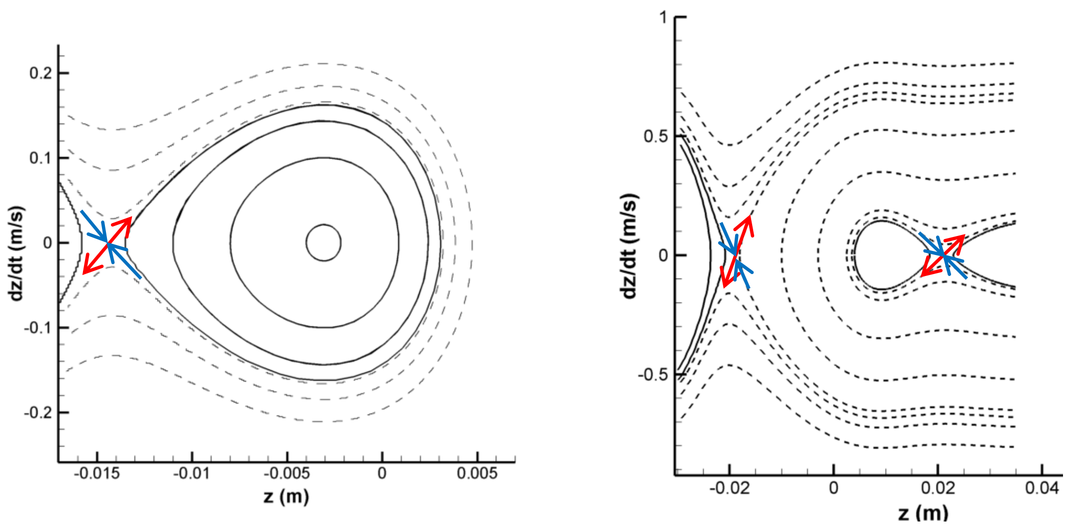

Fig. 8 – Phase space portraits in earth bound (left) and zero gravity (right) conditions.

The unstable equilibria in zero-gravity are of relevance because, irrespective of the presence or absence of gravity, it is at these positions that Joule heating in the droplet approaches local maxima – see Fig. 9. We will see shortly that strong coupling occurs at these positions. The gradient of the heating curve at the earthbound stable equilibrium is quite high - approximately 8 W/mm - which would suggest that even small amplitude oscillations could cause significant fluctuation in the temperature. This highlights the importance of eliminating axial instability when measuring the phase shift in the temperature oscillation.

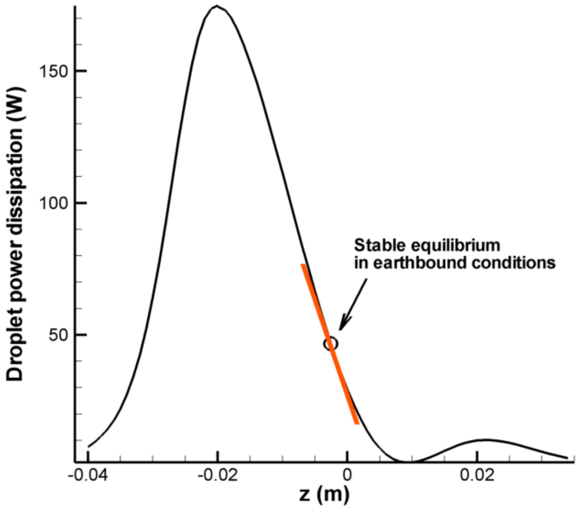

Fig. 9 – Time-averaged Joule heating as a function of the axial position of the spherical droplet (COMSOL).

3.3 Changes in the Circuit Impedance

In this section we investigate how the circuit impedance varies according to the position of the droplet on the symmetry axis of the coils. If a fixed voltage is maintained across the terminals of the excitation coil any oscillatory motion of the droplet could cause the current to wander slightly, implying the need for a small correction to the Lorentz force. To investigate this we follow an approach similar to that described in Iwai & Asai [7] and consider the levitator as an electrical circuit model of a transformer. In this model the excitation coil forms the primary winding and the droplet forms the secondary winding as shown in Fig. 10.

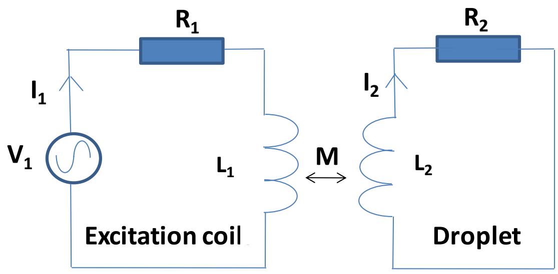

Fig. 10 – Electrical circuit model of the levitator.

From Kirchoff's voltage law, the following equations hold for each winding:

$$V_1 = (i\omega L_1 + R_1)I_1 + i\omega M\, I_2 \tag{6}$$

$$0 = (i\omega L_2 + R_2)I_2 + i\omega M\, I_1 \tag{7}$$

where I_i, V_i, R_i, L_i are the primary (i=1) and the secondary (i=2) currents, voltages, resistances, self-inductances respectively; M is the mutual inductance and ω is the angular frequency of the supply.

Eliminating I_2 from Eqns. 6 and 7 yields

$$V_1 = (R_1 + \Delta R_1)I_1 + i\omega(L_1 - \Delta L_1)I_1 \tag{8}$$

where

$$\Delta R_1 = \frac{\omega^2 M^2 R_2}{R_2^2 + \omega^2 L_2^2} \quad \text{and} \quad \Delta L_1 = \frac{\omega^2 M^2 L_2}{R_2^2 + \omega^2 L_2^2} \;. \tag{9}$$

Hence the circuit in Fig. 10 can be represented by Fig. 11 which shows *effective* values of inductance and resistance.

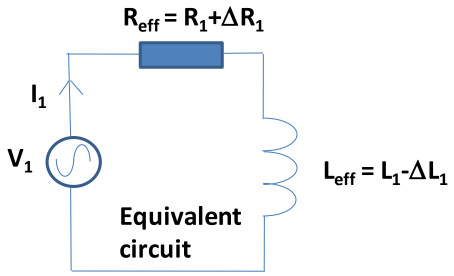

Fig. 11 – Equivalent electrical model.

Varying the *z*-position of the droplet affects the coupling *M* between the two circuits. The zero-gravity unstable equilibria are associated with local maxima in *M* where the coupling is strong due to the high flux linkage. Eqns. 8 and 9 indicate that increasing *M* increases the effective circuit resistance R_1+ΔR_1 but reduces the effective inductance L_1-ΔL_1. This result is intuitive because at the unstable equilibria the droplet experiences maximum Joule heating. Additionally, the streamlines of magnetic flux are distorted leading to a "bottleneck effect" which limits the amount of flux circulating around the coils. These effects become more pronounced as the frequency is increased due to intensification of the skin effect. Since the circuit impedance in the silicon droplet experiments [3,4] is dominated by the inductive reactance (due to the high frequency) the impedance will drop if the droplet moves near the zero-gravity unstable equilibria. If the circuit is voltage-driven this will cause an increase in the current.

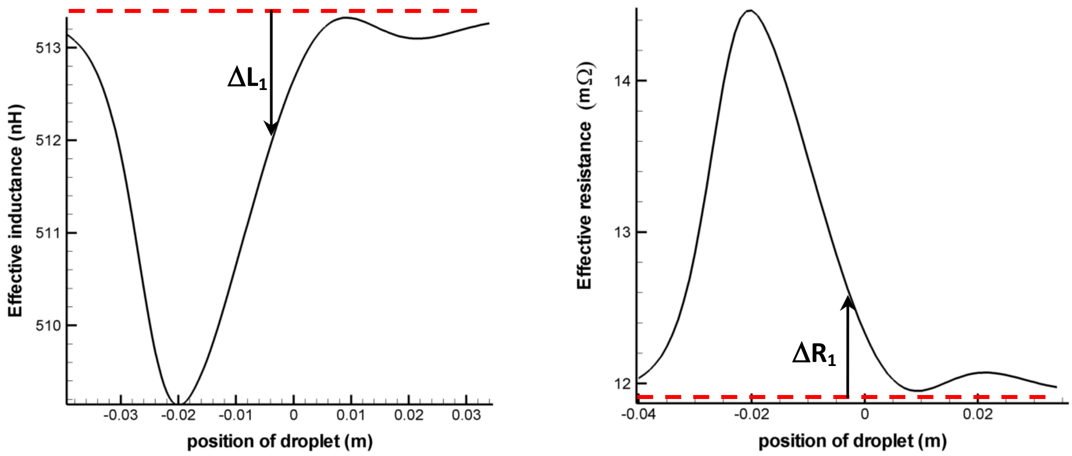

Fig. 12 – Effective inductance (L_{eff}) and effective resistance (R_{eff}) as function of *z*-position of droplet (COMSOL)

Fig. 12 shows the effective inductance and resistance of the levitator as a function of the axial position of the droplet. These graphs are obtained from COMSOL by computing the voltage V_1 required to impose the given current I_1 =375+0i (A) and applying Eqns. 8 and 9. In keeping with the previous remarks we see that the turning points occur at the zero-gravity equilibria. In the limit when the droplet lies infinitely far away from the coils the influence of the secondary circuit becomes negligible and we see that $L_{eff} \rightarrow L_1$ (=513.4 nH) and $R_{eff} \rightarrow R_1$ (=11.8 mΩ) (indicated by the dotted red lines). At 200 kHz, it is easily seen that $\omega L_{eff} >> R_{eff}$.

If a fixed peak voltage V_1=241.61V is maintained across the coil terminals and the droplet is positioned according to Fig. 1, a peak current of 375A flows in the coil (as discussed in Sec. 3.1). If the axial position of the droplet is slowly adjusted (maintaining the same voltage) the amplitude of the steady-state coil current I_1 will vary according to Fig. 13. The current I_1 is obtained from

$$I_1 = \frac{V_1}{|Z|} = \frac{241.61}{\sqrt{R_{eff}^2 + \omega^2 L_{eff}^2}}$$

where R_{eff} and L_{eff} are given by Fig. 12. The maximum current of 377.2 A which represents an incremental percentage change of 0.6% occurs at the zero-gravity unstable equilibrium (z = -0.02) where the impedance $|Z|$ is minimum.

The Lorentz force which acts on the droplet is obtained from the volume integral Re($\boldsymbol{J}$x$\boldsymbol{B}$*)/2. Since $\boldsymbol{J}$ and $\boldsymbol{B}$ both vary linearly with current the axial force will vary as the square of the current. Hence the adjusted terrestrial force F_z* is given by

$$F_z^* = \left[\left(\frac{I_1(z)}{375} \right)^2 F_z \right] - mg$$

where $I_1(z)$ is obtained from Fig. 13 and F_z coincides with the zero-gravity force curve in Fig. 7. Hence the terrestrial force correction ΔF_z is

$$\Delta F_z = \left[\left(\frac{I_1(z)}{375} \right)^2 - 1 \right] F_z \qquad .$$

There are five axial positions where ΔF_z = 0 which are shown in Fig. 13 (right). Three of these correspond to zero-gravity equilibria (at z =-0.02, 0.01, 0.02) where the force is independent of the current (and therefore requires no correction) and two of these correspond to positions where $I_1(z)$=375 A. At the reported stable equilibrium (z=-0.003) described in [4] the current I_1=375A since it is chosen as the reference. In addition, we find that I_1=375A at z = -0.031 since the effective inductance matches the value at z=-0.003 (see Fig. 12) and leads to the same impedance.

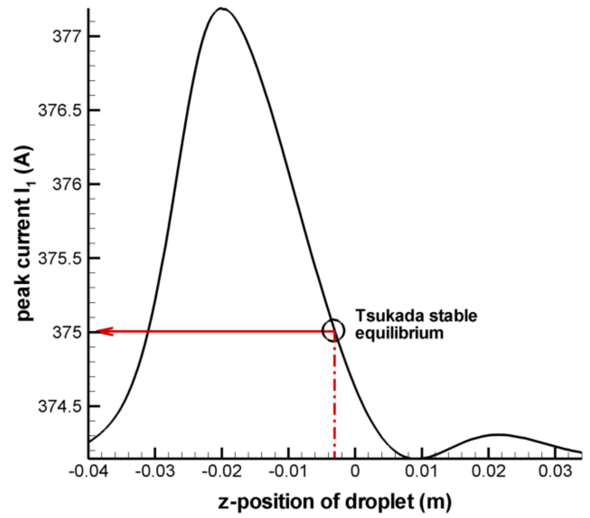

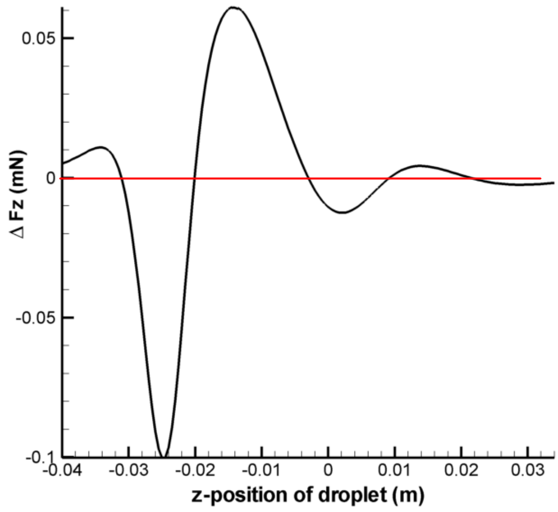

Fig. 13 – Peak current I_1 (left) and force correction ΔF_z (right) (COMSOL).

4. Numerical results using SPHINX

When the droplet is levitated in experimental conditions the heat generated from the induced eddy currents causes it to melt and deform. The results in this section, all produced using SPHINX, show (i) the more realistic shape assumed by the droplet in a typical experiment and (ii) the turbulent flow pattern and temperature field arising when the static magnetic field is very weak/absent.

While 375A is sufficient to achieve levitation of a droplet which is assumed to remain spherical, numerical simulations with SPHINX suggest that a higher current is necessary when the surface shape deformation is taken into account. This is because the changing geometry of the droplet will affect the force it experiences. As discussed in [8], current adjustment is often required in experiment to obtain stability. The plots of velocity and temperature (without laser heating and DC field) in Fig. 14 generated by SPHINX were obtained using a peak current of 530A in the excitation coil.[1] The increased current was used to avoid large amplitude centre-of-mass translational oscillations of the deformed droplet which would require long computational times to simulate. If no DC magnetic field is applied, intense turbulent flow develops in the interior of the droplet. Compared to the COMSOL plot of temperature (Fig. 5) where the flow was laminar and heavily damped by the strong DC magnetic field, the turbulence enhances the effective thermal diffusion and reduces the temperature variation throughout the droplet from 12° to just over 3°. The average temperature is about 85° lower due to the adjustment in operating conditions which makes the deformed droplet rest higher in the field where it experiences lower levels of Joule heating. Fluid velocities of 0.1 m/s are realised, making the Reynolds number of the order 10^4. In this scenario the droplet assumes the more realistic diamond shape with dimensions as indicated in Fig. 14. The effective turbulent viscosity, computed using the k-ω model is shown in Fig. 15. It is appropriate to note that neither COMSOL (without implementation of a turbulence model) nor the numerical model described by Tsukada [4] can simulate fluid flow in the non-laminar regime when the DC magnetic field is zero or moderately weak (<1T).

[1] While a current exceeding 375 A is necessary the particular choice of 530 A is arbitrary.

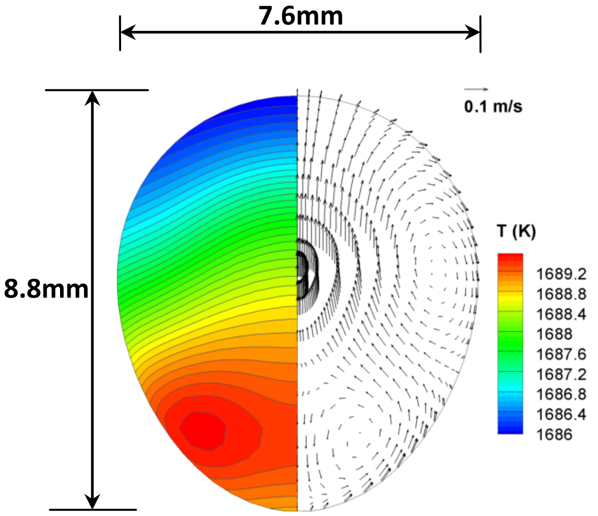

Fig. 14 – Temperature and velocity without DC field (SPHINX).

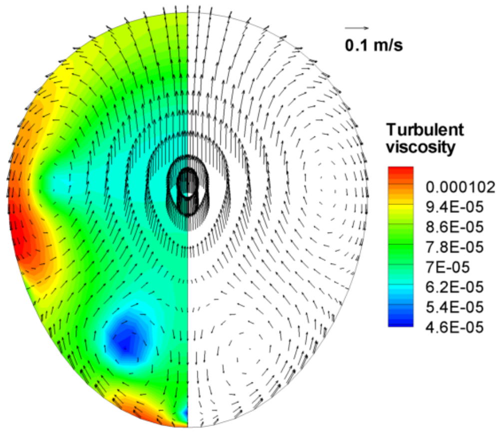

Fig. 15 – Effective turbulent viscosity without DC field (SPHINX).

We now consider what happens when the static magnetic field is gradually increased. At moderate field strengths when B_{dc}=1T, the flow intensity actually increases compared to the situation when B_{dc}=0 T. This is apparent from Fig. 16 which shows large-scale circulation velocities of 0.2 m/s. In this scenario the mean large-scale flow is readjusted in a pattern along the vertical DC magnetic field (see Figs. 14 and 16), the turbulence is damped by the magnetic field and the effective viscosity to reduced to a near- laminar value. Compared to Fig. 14 the temperature variation throughout the droplet has increased from 3° to 6° - presumably because the shift in the position of the vortices reduces convective heat transfer to the top of the droplet.

Further increasing the strength of the DC field more effectively suppresses the radial component of fluid velocity and decreases the average flow. Fig. 17 shows the velocity and temperature field when B_{dc}=5T where conditions approaching laminar flow and heat transfer are achieved. Thermo-capillary effects are noticeable on the surface of the droplet which are not easily damped by the action of the vertical DC magnetic field. The temperature variation throughout the droplet is 11° and velocities of around 0.006 m/s occur on the symmetry axis. This compares well with the COMSOL results in Fig. 5 and suggests that, while the average temperature in the droplet is lower due to the adjustment in shape and position the spatial distribution of T is similar to that obtained for a spherical droplet.

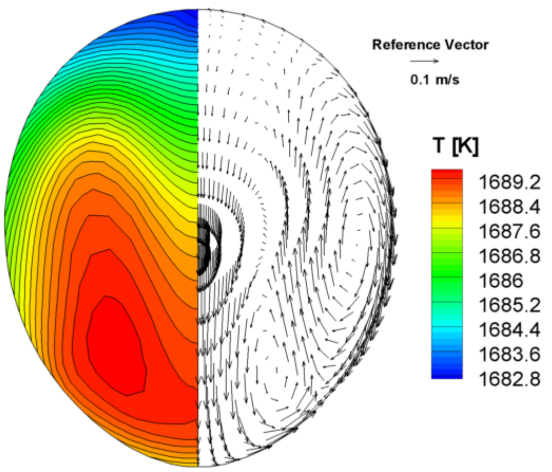

Fig. 16 – Velocity/temperature field when B_{dc}= 1 T. (SPHINX)

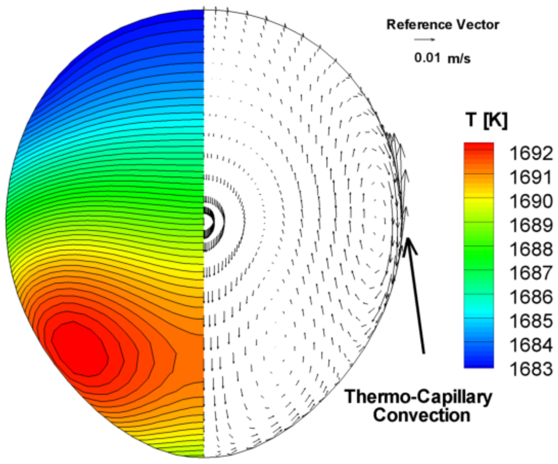

Fig. 17 – Velocity/temperature field when B_{dc}= 5 T. (SPHINX)

5. Conclusions

The results produced using COMSOL and SPHINX confirm the findings in [4] and indicate the importance of achieving stability when measuring the phase shift. Axial translational motion could cause significant fluctuation in the level of Joule heating and cause changes in the circuit impedance. Both these effects could disrupt the temperature modulation state.

The results produced by SPHINX indicate that, in the absence of a DC field, the levitated droplet is subject to large scale internal flow and small scale turbulence which enhances its heat transfer properties. The small-scale turbulence can be damped by introducing a DC field of moderate strength which could result in large-scale flow pattern adjustment and increased intensity. A sufficiently strong DC magnetic field damps both the flow and turbulence, resulting in conditions similar to laminar thermal diffusion. When a strong static magnetic field is applied, the SPHINX simulations reveal similar heat/flow patterns to those predicted by COMSOL but indicate the more realistic surface shape which the droplet will assume in a practical experiment.

6. References

[1] I. Egry, A. Diefenbach, W. Dreier, J. Piller (2001) , Inter. J. Therm. Phys., 22, 2, 569-578

[2] R. Wunderlich, H. Fecht (2005), Meas. Sci. Technol. 16, 402-416

[3] H. Fukuyama, H. Kobatake, K. Takahashi, I. Minato, T. Tsukada, S. Avaji (2007), Meas. Sci. Technol. 18, 2059-2066

[4] T. Tsukada, H. Fukuyama, H. Kobatake (2007), Int. J. Heat Mass Transfer 50, 3054-3061

[5] O. Widlund (2000), Modelling of magnetohydrodynamic turbulence, Ph.D. Thesis, Royal Institute of Technology, Stockholm, Sweden, ISSN 0348-467X

[6] V. Bojarevics, K. Pericleous (2003), ISIJ International, 43, 6, 890-898

[7] K. Iwai, S. Asai, 1995, Modelling Simul. Mater. Sci. Eng. **3,** 473-484

[8] H. Kobatake, H. Fukuyama, I. Minato, T. Tsukada, S. Avaji (2007), Applied Physics Letters 90, 094102

[9] V. Bojarevics, S. Easter, A. Roy and K. Pericleous. (2009) Levitated Liquid Droplets in AC and DC Magnetic Field. Proceedings International Symposium on Liquid Metal Processing and Casting, , Santa Fe, TMS, ed-s P.Lee, A.Mitchell, R.Williamson, pp. 319-326.

[10] COMSOL multiphysics (v. 3.5) www.comsol.com